Journal of Inflammation Research

Dovepress
open access to scientific and medical research

Open Access Full Text Article

ORIGINAL RESEARCH

Traditional Chinese Manual Therapy (Tuina) Improves Knee Osteoarthritis by Regulating Chondrocyte Autophagy and Apoptosis via the PI3K/AKT/mTOR Pathway: An in vivo Rat Experiment and Machine Learning Study

Zhen Wang[1,*], Hui Xu[1,2,*], Zheng Wang[1,*], Yu Wang[3,*], Jieyao Diao[1], Juntao Chen[1], Yuchen Xie[4], Lijuan Zhang[5], Miaoxiu Li[6], Yanqin Bian[7], Yunfeng Zhou[1]

[1]College of Acupuncture and Massage, Henan University of Chinese Medicine, Zhengzhou, People's Republic of China; [2]Tuina Department, The Third Affiliated Hospital of Henan University of Chinese Medicine, Zhengzhou, People's Republic of China; [3]College of Computer Science, Xidian University, Xian, People's Republic of China; [4]Tuina Department, Henan Provincial Hospital of Traditional Chinese Medicine, Zhengzhou, People's Republic of China; [5]Rehabilitation Department, Jiaozuo Coal Industry (Group) Co. Ltd. Central Hospital, Jiaozuo, People's Republic of China; [6]College of Acupuncture and Massage, Shanghai University of Chinese Medicine, Shanghai, People's Republic of China; [7]Orthopaedic Research Laboratory, University of California, Davis, CA, USA

*These authors contributed equally to this work

Correspondence: Hui Xu; Yunfeng Zhou, Email 15036065036@163.com; zyf5680198@126.com

Background: Knee osteoarthritis (KOA) is on the rise due to lifestyle changes, obesity, and aging, yet effective treatments are lacking. Traditional Chinese manual therapy (Tuina) is promising for KOA. However, its mechanism remains unclear.

Objective: This study aims to determine the effects of Tuina on a rat KOA model, focusing on the role of chondrocyte apoptosis and autophagy mechanisms.

Methods: KOA was induced in rats by intra-articular injection of L-cysteine-activated papain into the right knee. Thirty-six male Sprague Dawley (SD) rats were randomly divided into blank, model control, Tuina, and positive drug groups. Paw withdrawal threshold tests, knee joint swelling, and passive range of motion assessed knee behavior. Cartilage tissue cytology, cytokine contents, and the mRNA and protein expression of PI3K/AKT/mTOR signaling pathway components were analyzed using HE and TUNEL staining, ELISA, RT-qPCR, and Western blotting, respectively. In addition, we used machine learning methods to conduct a secondary analysis of the dataset from the in vivo experiments in rats to verify the findings.

Results: Tuina significantly relieved pain and joint swelling, and improved range of motion. Staining showed reduced articular cartilage destruction and apoptosis. Tuina reduced the serum levels of IL-1β, IL-17, MMP-3, and MMP-13. Tuina downregulated Bax, ULK1, Beclin-1, LC3-II/I and upregulated PI3K, AKT, mTOR, and BCL-2 in cartilage tissue. The machine learning results indicated an 83.33% accuracy for the prediction model, remaining stable through both uni- and multivariate analyses. Tuina yielded the best comprehensive efficacy on KOA as well as better rat behavior and PI3K/AKT/mTOR signaling pathway improvement effect than positive drugs, while its cytokine-reducing ability was comparable to that of positive drugs.

Conclusion: Tuina can alleviate cartilage tissue injury in KOA, relieve inflammation, and reduce chondrocyte apoptosis and autophagy, the underlying mechanisms of which may be associated with activation of the PI3K/AKT/mTOR signaling pathway.

Keywords: knee osteoarthritis, apoptosis, autophagy, tuina, PI3K/AKT/mTOR signaling pathway, in vivo experiment, machine learning

Introduction

Knee osteoarthritis (KOA) is a prevalent degenerative bone and joint disease marked by high clinical incidence, persistent duration, pain, and limited activity, significantly impacting middle-aged and older adults.[1–4] The global prevalence of KOA,

Received: 7 August 2024
Accepted: 12 September 2024
Published: 17 September 2024

ranging from 4.2–15.5%, increases with age,[5] driven by lifestyle alterations, high obesity rates, and population aging, placing a substantial burden on individuals and healthcare systems.[6,7] While diverse treatments like oral medications, intra-articular injections, surgeries, and physical therapy are employed for KOA management, they often strain finances, and may have adverse gastrointestinal, cardiovascular, and renal side effects.[8,9] Therefore, seeking a cost-effective KOA intervention strategy with evident efficacy and a clear mechanism is paramount in contemporary research.

Tuina therapy has gained prominence in KOA treatment due to its multi-target regulation, significant efficacy, and minimal side effects.[10–13] Our prior clinical investigations attest to the efficacy of Tuina in enhancing knee tenderness thresholds, relieving pain, and improving functional capacities.[14–16] However, the mechanism of its action in KOA remains unclear, necessitating further empirical investigation. Apoptosis and autophagy, closely linked to chondrocyte survival maintain cell health and tissue homeostasis.[17] Dysregulation of these processes disrupts the synthesis and metabolism of chondrocytes, resulting in reduced secretion of extracellular matrix that maintains normal cartilage function, and ultimately accelerated cartilage destruction. Apoptosis and autophagy provide new targets for preventing, diagnosing, and treating KOA.[18,19] Previous studies on the mechanisms associated with Tuina therapy for KOA have tended to focus of reducing inflammatory responses, with only a single study mentioning chondrocyte apoptosis.[20] Additionally, the mechanism through which Tuina regulates upstream molecules to promote chondrocyte apoptosis and autophagy remains unclear.

Various signaling pathways regulate apoptosis and autophagy. With the continuous development of traditional Chinese and modern medicine, the PI3K/AKT/mTOR signaling pathway has gradually become a research hotspot in KOA.[21] This pathway is involved in key cellular processes, including proliferation, apoptosis, and autophagy, which play essential roles in maintaining cartilage homeostasis.[22–24] Notably, the influence of this pathway on chondrocyte survival and function makes it an ideal target for therapeutic interventions aimed at retarding or reversing cartilage degeneration in KOA. However, its interplay with Tuina therapy in KOA remains uncharted.

Animal experiments provide significant advantages in studying diseases mechanisms and action mechanisms. However, they only reflect the improvement of treatment measures on a single outcome indicator and cannot predict the overall regulatory effect or the synergistic correlation between indicators, thereby limiting the extrapolation of research results.[25] The advent of machine learning technology in recent years has revolutionized medical research by addressing these limitations. With its robust data processing and pattern recognition capabilities, machine learning can predict and analyze complex biological data, overcoming the data interpretation and prediction challenges of animal experiments.[26,27] Among machine learning methods, the random forest algorithm is widely used for extracting rules and trends from extensive experimental data.[28] It evaluates the importance of each indicator for prediction outcomes, and optimizes detection indicator selection. Moreover, the random forest algorithm assesses treatment effectiveness, providing valuable validation and complementing findings from animal experiments.

Therefore, this study aims to investigate whether Tuina can regulate apoptosis and autophagy, protect chondrocytes in KOA, and delineate associated signaling pathways through in vivo experiments and machine learning. It also aims to provide theoretical references and evidence-based support for Tunia use in KOA in clinical practice.

Materials and Methods

Figure 1 illustrates the specific process of this study. Initially, in vivo experiments were conducted in rats, encompassing KOA model preparation, group therapy, cartilage staining, behavioral and serum detection, mRNA and protein expression analysis, and statistical data analysis. Subsequently, data from the rat in vivo experiment was utilized as the dataset for machine learning secondary analysis. This analysis involved data preprocessing, random forest model construction, feasibility and importance analysis, and efficacy evaluation.

Vivo Experiment in Rats

Animals and Groups

Thirty-six male Sprague–Dawley (SD) rats (weighing 280–320g, aged 8–9 weeks) were purchased from Beijing Vital River Laboratory Animal Technology Co., Ltd. [Eligibility Number: SCxK (Jing) 2021–0006]. They were

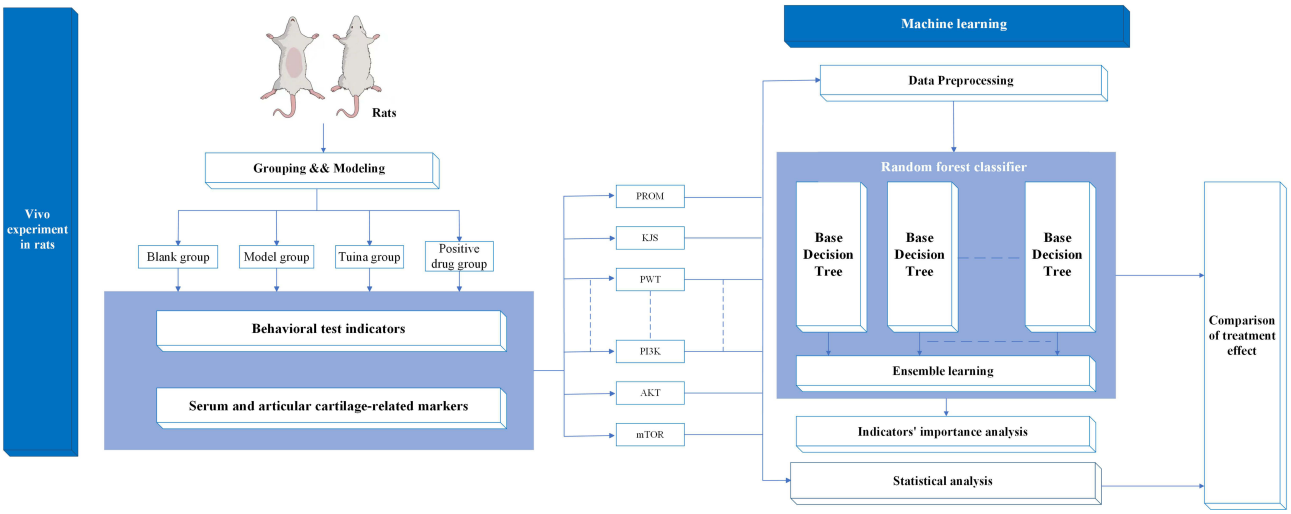

Figure 1 Flow chart of in vivo experiments and machine learning study.

individually housed at 20°C±2°C with 40–50% humidity, provided standard pellet feed and drinking water ad libitum, and maintained on a 12-hour light/dark cycle with regular cage cleaning and disinfection. All experiments were performed using procedures approved by the Committee of Animal Experimental Center of Henan University of Chinese Medicine (approval number: IACUC-202309024). Instrument and reagent details are provided in Supplementary Table 1.

After 1 week of adaptive feeding, the rats were randomized into the blank (n=9) and the model control groups (n = 27) using a random number table method. After molding, one rat from each group was randomly selected for model evaluation. The remaining model control rats were randomly divided into three groups: model control (n = 8), Tuina (n = 8), and positive drug (n = 8).

Establishment of a Rat Model of KOA

A rat model of KOA was induced by intra-articular injection of L-cysteine-activated papain.[29,30] The solution preparation steps are as follows: papain was dissolved in sterile physiological saline to a concentration of 4%, and L-cysteine was dissolved in sterile physiological saline to a concentration of 0.03 mol/L. Papain (4%) was mixed with L-cysteine (0.03 mol/L) at a 2:1 ratio and incubated at room temperature for 30 minutes.

All 27 animals were anesthetized by an intraperitoneal injection of 3% sodium pentobarbital at 3 mg/100 g after 12 hours of fasting. The rat was then placed on the operating table, and the hair on the right knee was scraped and disinfected with iodophor. The knee joint of the rat was bent at 45°, and 0.2 mL L-cysteine-activated papain solution was slowly injected into the joint cavity with the outer edge of the patellar tendon under the patella as the injection point. The procedure described above was strictly followed for three injections (on the 1st, 4th, and 7th days). Having received three injections, the rats were assessed for behavioral changes, such as pain level, knee swelling, and joint mobility, using the Lequesne MG rating scale,[31] with a score greater than 4 being taken to be indicative of successful modeling. In addition, one rat in each group was randomly selected for hematoxylin and eosin (HE) staining, and the degree of knee cartilage injury was evaluated using the Mankin score.[32] A Mankin score equal to or greater than 6 was considered to indicate successful KOA model construction.

Intervention Methods

Tuina group: Rats were fixed on an immobilized rat plate, and the right knee treatment site was exposed. The point selection, operation method, frequency and cycle of Tuina intervention were based on reference to the Chinese national normative textbook "Therapeutics of Chinese Tuina.[33]"The procedure followed in the Tuina group are as follows: (1) press and kneading manipulation: ①Application area: Select a total of 4 acupoints on the right hind limb of rats, including "Neixiyan" (EX-LE4), "Dubi" (ST35), "Yinlingquan" (SP9), and "Yanglingquan" (GB34) (Figure 2, Table 1). Locate the acupoints according to the principles of acupoint positioning in "Map of Acupuncture and Moxibustion

Figure 2 The diagram of the acupoints in rats.

Acupuncture Points for Laboratory Animals.[34]" ②Tuina manipulation: Press and kneading manipulation is done on the four acupoints for 2 minutes each. Place the performer's thumb on the selected acupuncture points to perform rhythmic pressing and kneading, moving the skin and subcutaneous tissue together in a circular motion. ③Manual quality control: Use finger pressure recordings (units in Newton) to ensure consistent intensity and frequency of manipulation. Keep the intensity between 3–5 N and the frequency at 60 times/min. (2) Knee flexion and extension: Bend the rat's knee joint, then press the thumb of one hand on the lower edge of the patella and extend the knee joint of the rat while exerting

Table 1 The Acupoint Position of Rat Tuina Operation

Acupoint Name	Acupoint Location	Topographic Anatomy
Neixiyan (EX-LE4)	Ichannel tropism: Extra Nerve Points. Location: located in the knee, under the patella and in the medial depression of the patellar ligament.	The superficial layer is covered with the infrapatellar branch of the saphenous nerve and the anterior cutaneous branch of the femoral nerve. The deeper layers contain the arterial and venous network of the knee joint.
Dubi (ST35)	Ichannel tropism: Stomach Meridian of Foot-Yangming. Location: located in the depression of the lateral patellar ligament of the knee.	There is a network of arteries and veins of the knee joint. There are peroneal lateral cutaneous nerve and articular branch of common peroneal nerve.
Yinlingquan (SP9)	Ichannel tropism: Spleen Meridian of Foot-Taiyin. Location: located on the medial side of the calf, in the depression between the medial condylar margin of the tibia and the medial tibia, between the posterior margin of the tibia and the gastrocnemius, at the origin of the soleus muscle.	Anteriorly there is the saphenous vein, the uppermost artery of the knee, and at the deepest level the posterior tibial artery and vein; and there is the present trunk of the medial cutaneous nerve of the calf, and at the deepest level the tibial nerve.
Yanglingquan (GB34)	Ichannel tropism: Gallbladder Meridian of Foot-Shaoyang. Location: located on the lateral side of the calf, in the anterior lower depression of the fibula head.	Subcutaneous distribution of the biceps femoris, lateral artery and vein below the knee and superficial and deep peroneal nerves.

force. Repeat this 10 times. Apply the manipulation daily for 2 weeks. In order to reduce the influence of confounding factors, only a single therapist carried out the entire treatment of all rats in the Tuina group.

Positive drug group: Celecoxib was dissolved in normal saline, and a solution with a 2.4 mg/mL concentration was prepared. Rats in the celecoxib group were administered 10 mL/kg celecoxib solution once daily for 2 weeks.

Blank and model control groups: The blank and model groups were administered 1 mL/kg/d of normal saline continuously for 2 weeks.

Sampling

After 12 hours of diet prohibition, the rats were weighed. After confirming muscle tension, articular cartilage samples were collected following blood collection.

Blood collection involved anesthetizing rats, fixing their limbs, disinfecting their abdomen, and making an inverted "T" incision to access the inferior vena cava. A 20° tilted needle insertion into the inferior vena cava, connection to a vacuum coagulation-promoting collection vessel, and in vitro heart compression accelerated blood collection. After standing for 30 minutes, the blood was stratified and centrifuged at 3000 rpm for 10 minutes. Yellow translucent serum was obtained and placed in a cryostorage tube at −80°C for enzyme-linked immunosorbent assay detection.

After blood collection, the rats were quickly placed on ice, exposing their right knee joint. The medial articular cartilage of the tibial plateau of the right knee joint and the medial condylar cartilage of the femur were removed and divided into two parts. One part was frozen at −80°C for Western blot and reverse transcription-polymerase chain reaction analysis. The other part was fixed in 4% paraformaldehyde solution for 48 hours for hematoxylin and eosin (HE) and TUNEL staining.

Paw Withdrawal Threshold Tests (PWT)

The severity of joint pain was quantitatively evaluated based on the PWT using an Electric Von Frey. The rats were individually placed in metal cages, which allowed full access to the paws, and were acclimated for at least 30 minutes before the test. After the rats were quieted, the probe was applied perpendicularly to the mid-plantar surface of the right hind paw to evaluate the withdrawal threshold. Data were recorded on the display screen until the force elicited a nocifensive response (ie, paw lifting and jumping). This procedure was repeated thrice with an inter-stimulus interval of 3 minutes. The mean values of the three tests were used for statistical analyses. The PWT test was performed after modeling and after 2 weeks of treatment.

Measurement of knee joint swelling (KJS) and passive range of motion (PROM).

The transverse diameter of the right knee was measured using a sliding caliper, and the horizontal distance between the highest left and right points of the knee joint, flexed at 90°, was measured and recorded.

The passive motion of the knee joint on the affected side of the rats in each group was measured using a medical angle ruler. The specific operation was as follows: the femur on the affected side of the rat was aligned parallel to the fixed ruler end of the protractor, and the joint activity axis was relative to the protractor axis. The rats' knee joints were passively extended and flexed while the angle ruler moved with the tibia. The maximum extension angle was recorded when the knee joint reached its fullest extension, and the maximum flexion angle was recorded at its maximum flexion. Joint passive motion=maximum flexion angle - maximum elongation angle, measured thrice for each rat and averaged.

Knee joint swelling and PROM were measured after modeling and 2 weeks of treatment.

HE Staining and Mankin Score

Paraffin was sliced and placed in xylene I and II liquid, anhydrous ethanol I and II liquid, 95% ethanol by volume, 90% ethanol by volume, 80% ethanol by volume and distilled water. It was placed in a modified Lillie-Mayer hematoxylin staining solution for 5 minutes, differentiated by hydrochloric acid ethanol, with distilled water turning blue, and put in an eosin staining solution for 5 minutes. The rats were rinsed, dehydrated, made transparent, and sealed under a light microscope for observation at 200x magnification. Cartilage staining of three rats per group was scored by three independent researchers using the Mankin score to assess the degree of knee cartilage injury.

TUNEL Staining

Paraffin sections were dewaxed in water, placed in xylene I and xylene II for 20 minutes each, anhydrous ethanol I and II for 5 minutes each, and 75% alcohol for 5 minutes, and then rinsed with running water. The tissue was covered with protease K working liquid, incubated at 37°C for 15–30 minutes, and then washed in PBS thrice for 5 minutes each time. The tissue was covered with the film-breaking working liquid, incubated at room temperature for 20 minutes, and then washed in PBS thrice, 5 minutes each time. Buffer was added and incubated at room temperature for 10 minutes. After preparing the labeling solution, an appropriate amount of reaction solution was added according to the tissue size. The specimen was incubated at 37°C and away from light for 1 hour and then washed with PBS 4 times, 5 minutes each time. DAPI dye solution was added and incubated for 10 minutes at room temperature and washed with PBS thrice for 5 minutes each time. The tablets were sealed after an anti-fluorescence quencher was added. The nuclei of apoptotic cells showed red fluorescence, and the nuclei of DAPI-stained cells showed blue fluorescence when observed and captured by fluorescence microscopy under dark conditions. The cartilage from rats in each group was stained, and the red-positive area and red area density were calculated by three independent researchers to determine the degree of chondrocyte apoptosis in the knee joint.

Measurement of IL-6, IL-17, MMP-3, and MMP-13 Levels by ELISA

Serum samples from each group were prepared per the above method, re-dissolved in an appropriate amount of distilled water by vortexing, and the standard product was mixed 1:1 with standard diluents to generate a standard curve with the highest concentration. The detection antibody, detection buffer, and sample were added to the standard product holes and sample holes according to the manufacturer's instructions; enzymes, incubation, and plate washing were added, and the color-developing substrate TMB was added under dark conditions to allow incubation at room temperature for 5–30 minutes. Lastly, 100μL termination solution was added to each well, the color changed from blue to yellow after mixing, and the OD value at 450 nm wavelength was measured within 30 minutes by enzyme labeling instrument. The concentration was calculated and exported to an Excel table.

Reverse Transcription-Quantitative Polymerase Chain Reaction (RT-qPCR)

RT-qPCR was used to detect the mRNA expression levels of PI3K, AKT, BCL-2, Bax, mTOR, ULK1, Beclin-1, LC3-II, LC3-I in cartilage tissues. The methods and procedures were as follows: the cartilage tissue was ground in liquid nitrogen, 1 mL of RZ lysate was added to every 50 mg of tissue, and homogenized with a homogenizer. The homogenized sample was placed at 15–30°C for 5 minutes, 200μL chloroform was added, the tube cover was closed, and the sample was violently shaken for 15 seconds. The sample was placed at room temperature for 3 minutes and centrifuged at 12000 rpm at 4°C for 10 minutes. The centrifuged water phase was transferred to a new tube, 0.5x the volume of anhydrous ethanol was slowly added, mixed, transferred to adsorption column CR3, centrifuged at 12000 rpm for 30 seconds at 4°C, followed by 500μL of deproteinizing solution and bleaching solution, centrifuged at 12000 rpm for 30 seconds at 4°C, and the waste liquid was discarded. CR3 was put into a collection tube, and 50μL of RNase-Freedd H_2O was added, with the tube placed at room temperature for 2 minutes, and then centrifuged at 4°C for 12000rpm for 2 minutes.

After detecting mRNA purity and concentration using the ultra-micro nucleic acid analyzer, a reverse transcription reaction was performed: 2μLRNA was amplified by PCR, and a 20μL reverse transcription reaction system was configured. The amplification conditions involved enzyme activation at 95°C for 5 minutes in one cycle, denaturation at 95°C for 5 seconds, annealing at 60°C for 10 seconds, and extension at 72°C for 25seconds, repeated for 40 cycles, using GAPDH as the internal parameter. The relative expression of each gene was calculated using 2-ΔΔCt. Each experiment was repeated thrice. The primer sequences are listed in Table 2.

Western Blot Analysis

Western blotting was used to detect the protein expression levels of PI3K, AKT, BCL-2, Bax, mTOR, ULK1, Beclin-1, LC3-II, and LC3-I in the articular cartilage tissue of rats in each group. The methods and procedures were as follows: a total protein extraction kit was used to extract protein, BCA concentration was determined, the gel was prepared

Table 2 PCR Primer Sequences for Target Gene

Primers	Forward (5′–3′)	Reverse (5′–3′)
PI3K	CTGCTGCAAAACCCCATCAC	AGCGGTGGTCTATCAACAGC
AKT	ATGGACTCAAACGGCAGGAG	AGCACCTGAGTTGTCACTGG
BCL-2	GGTGAACTGGGGGAGGATTG	AGAGCGATGTTGTCCACCAG
Bax	GATCGAGCAGAGAGGATGGC	GTTGTTGTCCAGTTCATCGCC
mTOR	CACCAAGGCCTAATGGGGTT	CAACAACGGCTTTCCACCAG
ULK1	TACACACCCTCTCCCCAAGT	GTGCTCAGGCACAGAGGAG
Beclin-1	AGGAGAGAGCCAGGAGGAAG	GACACCATCCTGGCGAGTTT
LC3-II	GAAGACCTTCAAACAGCGCC	ATCACTGGGATCTTGGTGGG
LC3-I	AAGACCGGTCAGAAGCCATC	AGCAAGTGTGGACAGAGACG
GAPDH	TGATGCCCCCATGTTTGTGA	TTCTGAGTGGCAGTGATGGC

according to SDS-PAGE kit instructions, electrophoresis buffer was added after sample loading, and the sealing solution was placed in the sealing solution for 2 hours after transfer. The sealed PVDF membrane was placed in diluted primary antibody incubated in a shaking bed at 4°C overnight, and the primary antibody was recovered and washed with 1×TBST thrice. The washed membrane was incubated slowly for 1 hour on a secondary antibody (1:5000) shaking bed for 5 minutes and then washed thrice with TBST for 5 minutes each time. The protein side of the PVDF membrane was put into an ECL development solution for full reaction, soaked for 1–2 minutes, exposed, and developed on the machine. Finally, ImageJ software was used to analyze the relative content of protein expression.

Statistical Analysis

SPSS 26.0 and GraphPad Prism (version 8.0) software were used for statistical analysis and image capture. All data were expressed as mean±standard error of the mean. One-way analysis of variance was used to compare multiple groups, whereas the least significant difference method was employed for two-way comparisons between multiple groups. Bonferroni's post hoc test was used to compare multiple columns. Statistical significance was set at $P < 0.05$ (two-tailed).

Machine Learning

Data Sets and Preprocessing

We selected 20 intra-experimental indicators as input features for the machine learning model. These variables included behavioral measures (PWT, knee swelling, passive range of motion), staining measures (Mankin score, red positive area and red area density), cytokine measures (IL-1β, IL-17, MMP-3 and MMP-13), and PI3K/AKT/mTOR signaling pathway indicators (PI3K, AKT, mTOR, BCL-2, Bax, Beclin1, ULK1, LC3I, LC3II and LC3II/I). The behavioral indicators were labeled after modeling and treatment, while the PI3K/AKT/mTOR pathway indicators were labeled by mRNA and protein expression.

Text labels in the in vivo experimental data were converted into digital labels using one-hot encoding, and the dataset was normalized. The selected features were then analyzed to simplify the number of features and remove inappropriate ones, improving the stability and robustness of the model training.

Model Construction

The sklearn. ensemble tool in python 3.12.3 is utilized to construct a random forest model, consisting primarily of individual decision trees and ensemble integration.[35] Each decision tree includes root nodes, inner nodes representing decision rules, and leaf nodes indicating the final prediction outcomes. Starting from the root node, the dataset is recursively partitioned until a stopping condition is met, such as reaching maximum depth, all data points belonging to the same category, or having too few data points, resulting in multiple weak classifiers.[36] Segmentation criteria such as information entropy, information gain, gain rate or Gini impurity are used to determine partition points. The predictions

from basic decision trees constructed with different data subsets and segmentation criteria undergo ensemble decision processing. A strong classifier is then formed through weighted voting to determine the final classification results.[37,38]

Model Evaluation

Initially, the random forest model's performance is assessed using accuracy, the F1 metric, and the Kappa coefficient. Accuracy represents the proportion correctly classified samples to the total samples in the test set, commonly used in classification tasks.[39] The F1 metric and Kappa coefficient serve as supplementary measures to evaluate the consistency between classification and actual results.[40] We used a confusion matrix to comprehensively evaluate the model performance. The confusion matrix rows and columns represented the real and predicted categories, respectively, while each cell recorded the sample number corresponding to the actual combination with the predicted category. Furthermore, we normalized the confusion matrix and drew a visual matrix image.

Additionally, to evaluate the rationality and relative importance of selected indicators in this animal experiment, we categorized the rat dataset into four groups. We analyzed each indicator's rationality and importance based on the information entropy gain observed basic decision tree construction, considering its impact on the rat KOA.

Lastly, we selected the top ten most important experimental results from rats in the blank and model groups were selected as the training dataset. Rats treated with massage and drugs were tested using the model. Forest integration employed a majority voting method to evaluate the recovery effect on normal rats in each group after treatment. Two levels of efficacy evaluation were conducted for each indicator: overall efficacy analysis of Tuina on KOA and comprehensive effects analysis on type of index (behavioral, staining, cytokine and PI3K/AKT/mTOR signaling pathway-related indexes).

Results

Effects of Tuina on the PWT Tests, KJS and PROM in KOA Rats

This study initially investigated the effects of Tuina on PWT, knee joint swelling, and PROM. As depicted in Figure 3A–C, results demonstrated significant differences between each group and the blank group post-modeling ($P<0.05$), suggesting successful construction of the rat model of KOA.

Post-treatment, As depicted in Figure 3D–F, the Tuina and positive drug groups significantly improved in PWT and knee joint swelling compared to the model group ($P<0.05$). Tuina and celecoxib were equally effective in improving PWT ($P>0.05$), and the Tuina group was superior to the positive drug group in reducing swelling ($P<0.05$). Compared with the model group, the positive drug group had no significant effect on PROM ($P>0.05$), while Tuina treatment significantly improved PROM ($P<0.05$).

Histopathological Changes in Articular Cartilage and Mankin Sore

As shown in Figure 4A, HE staining showed that in the blank group, articular cartilage exhibited smooth surfaces, normal chondrocyte morphology, and clear structural integrity of the tide line. Conversely, the model group showed significant cartilage defects, chondrocyte necrosis and dissolution, reduced number, and irregular distribution of chondrocytes with an unclear tide line. Compared with the model group, the surface of articular cartilage in the Tuina group was smooth and the shape was complete. The chondrocytes were arranged regularly and distributed evenly in the matrix. The cluster of cells was visible, the number of cells was significantly increased, and the cartilage matrix was fully stained; however, the tide line was slightly incomplete. In the positive drug group, there was a moderate increase in chondrocytes in the articular cartilage, with partially deformed cartilage cells, smaller cracks on the surface of the cartilage and slightly uneven staining of the cartilage matrix.

To observe changes in the cartilage tissue in each group more accurately, the Mankin score was used for quantitative evaluation. As shown in Figure 4B, the Mankin score in the model group was significantly higher than that in the blank group ($P<0.05$), indicating the successful establishment of the KOA model. The Tuina and positive drug groups exhibited Mankin scores that were significantly lower than those of the model group ($P<0.05$). In addition, Mankin scores in the Tuina group were lower than those in the positive drug group ($P<0.05$), suggesting that Tuina significantly improved cartilage injury in KOA.

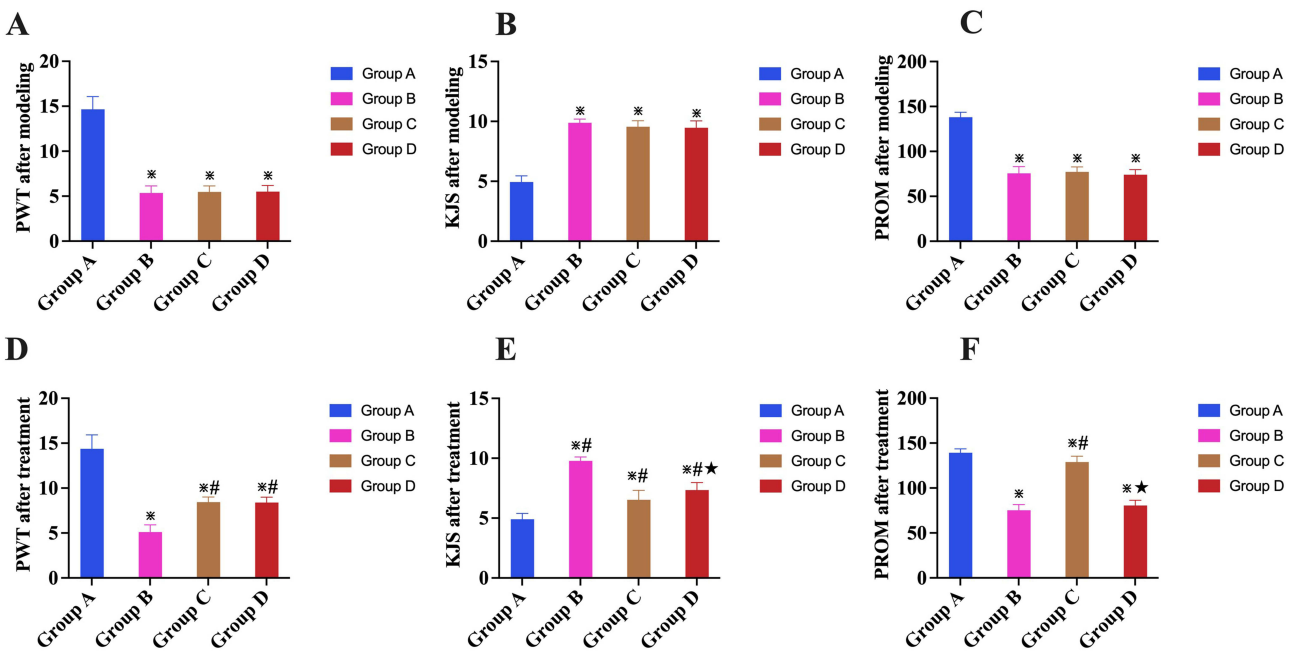

Figure 3 Effect of Tuina on behavioral indicators of the knee joint in KOA rats.
Notes: (**A**–**C**), PWT tests, KJS and PROM after modeling of KOA rats in each group; **(D**–**F**), PWT tests, KJS and PROM after treatment. Group A, blank group; Group B, model control group; Group C, Tuina group; Group D, positive drug group. ※ Compared with group A, P<0.05; # Compared with group B, P<0.05; ★ Compared with group C, P<0.05.
Abbreviations: KOA, knee osteoarthritis; PWT, Paw withdrawal threshold; KJS, knee joint swelling; PROM, passive range of motion.

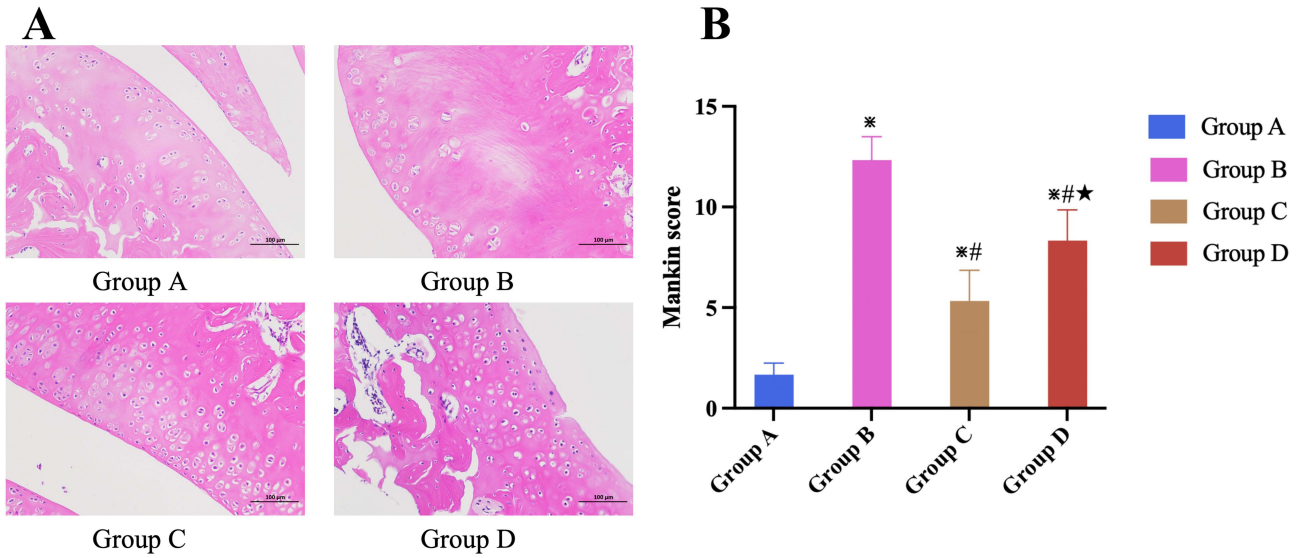

Figure 4 (**A**) Observation results of HE stained knee cartilage of rats in each group under light microscope. Scale, 200μm. (**B**) Mankin score of chondrocytes in each group.
Notes: Group A, blank group; Group B, model control group; Group C, Tuina group; Group D, positive drug group. ※ Compared with group A, P<0.05; # Compared with group B, P<0.05; ★ Compared with group C, P<0.05.

TUNEL Staining Assessment

Figure 5A shows the results of the TUNEL staining of the cartilage tissue in each group. To observe chondrocyte apoptosis in each group, the red-positive area and red area density were used for quantitative evaluation. As shown in Figure 5B–C, compared with the blank group, the red-positive area and red area density of chondrocytes in the model group increased (P<0.05). The red-positive area and red area density of chondrocytes in the Tuina and positive drug

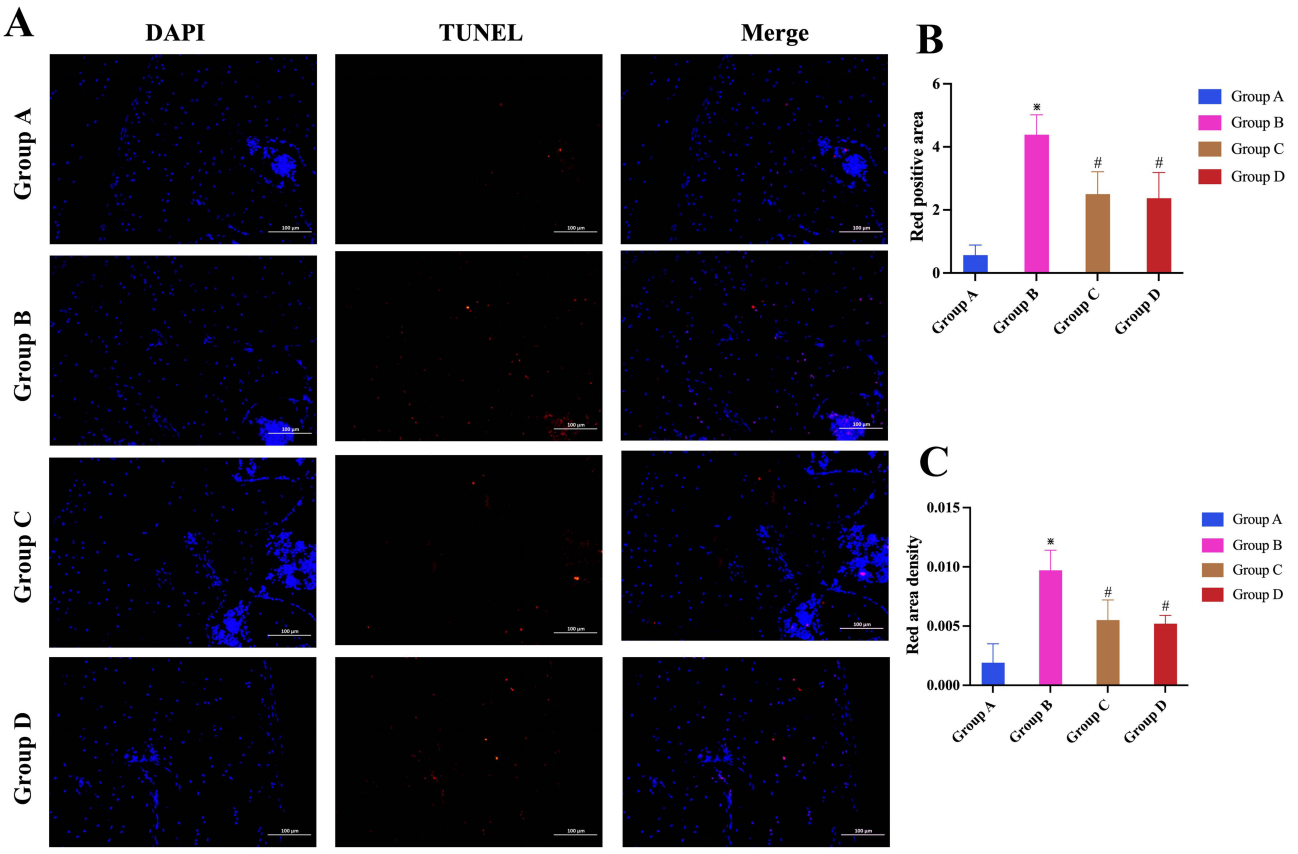

Figure 5 (**A**) Observation results of Tunel staining of cartilage tissue in each group. Scale, 100μm. Red positive area (**B**) and red area density (**C**) of chondrocytes in each group.
Notes: Group A, blank group; Group B, model control group; Group C, Tuina group; Group D, positive drug group. ※ Compared with group A, P<0.05; # Compared with group B, P<0.05.

groups decreased (P<0.05). Moreover, there was no statistically significant difference in the red-positive area and red area density between the Tuina and positive drug groups (P>0.05), indicating a comparable ability to improve chondrocyte apoptosis between the two groups.

Effects of Tuina on Serum Inflammatory Factors and Matrix Metalloproteinases in KOA Rats

As shown in Figure 6, the levels of IL-1β (Figure 6A), IL-17 (Figure 6B), MMP-3 (Figure 6C), and MMP-13 (Figure 6D) in the model group were significantly higher than those in the normal group (P<0.05). The levels of IL-1β, IL-17, MMP-3, and MMP-13 in the model group were higher than those in other treatment groups (P<0.05). Within the treatment groups, the Tuina group had the lowest levels of MMP-3 and MMP-13, followed by the positive control group (P<0.05). However, the two groups had no significant differences in IL-1β and IL-17 levels (P>0.05).

Effects of Tuina on the Expressions of PI3K/AKT/mTOR Signaling Pathway-Related mRNAs in Knee Cartilage Tissues of KOA Rats

As shown in Figure 7, the relative mRNA levels of PI3K, AKT, mTOR, BCL-2, and LC3I were the lowest. The relative mRNA levels of Bax, Beclin1, ULK1, LC3II, and LC3II/I were the highest in the cartilage tissues of the model control group, with significant differences compared to the normal group (P<0.05). Compared with the model group, the Tuina and positive drug groups exhibited significantly increased mRNA levels of PI3K, AKT, and BCL-2 and decreased mRNA levels of Bax (P<0.05). Compared with the model control and positive drug groups, the relative mRNA levels of mTOR and LC3I were notably elevated in the Tuina group (P<0.05), whereas the relative mRNA levels of Beclin1, ULK1,

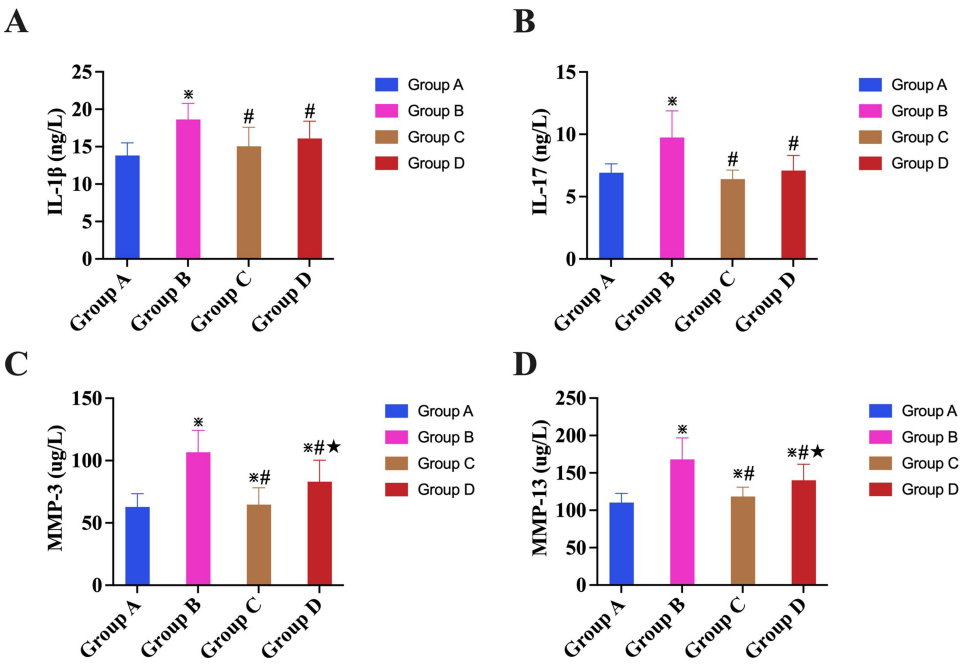

Figure 6 Effects of Tuina on the serum inflammatory factors and matrix metalloproteinases in KOA rats. Levels of IL-1β (**A**), IL-17 (**B**), MMP-3 (**C**) and MMP-13 (**D**) in serum of KOA rats in each group.
Notes: Group A, blank group; Group B, model control group; Group C, Tuina group; Group D, positive drug group. ※ Compared with group A, P<0.05; # Compared with group B, P<0.05; ★ Compared with group C, P<0.05.

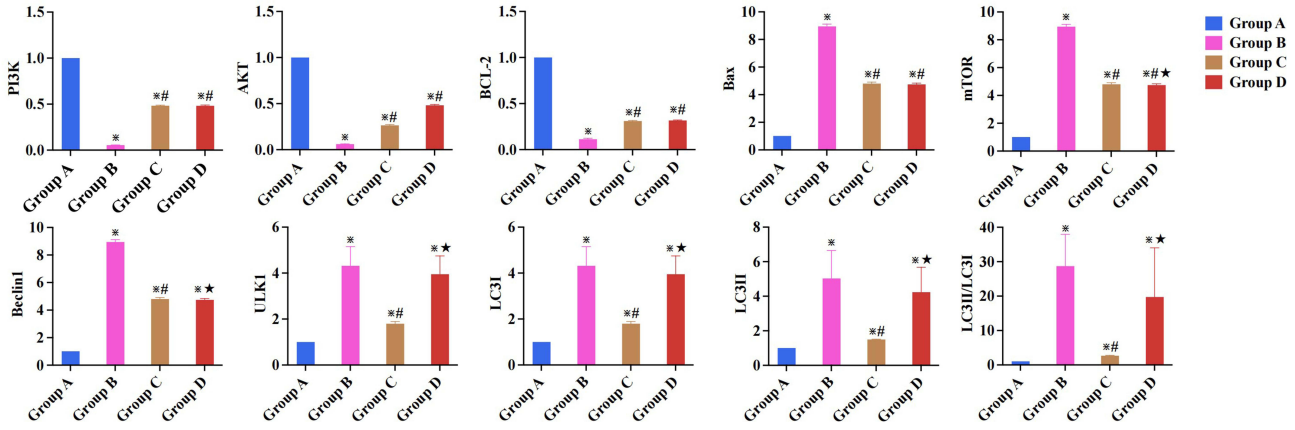

Figure 7 Effects of Tuina on the Expressions of PI3K/AKT/mTOR Signaling Pathway-Related mRNAs in Knee Cartilage Tissues of KOA Rats.
Notes: The ordinate is the relative expression of mRNA of each indicator. Group A, blank group; Group B, model control group; Group C, Tuina group; Group D, positive drug group. ※ Compared with group A, P<0.05; # Compared with group B, P<0.05; ★ Compared with group C, P<0.05.

LC3II, and LC3II/I were reduced (P<0.05). Regarding the regulation of mTOR, Beclin1, ULK1, LC3I, LC3II, and LC3II/I, the positive drug group showed no significant effect compared with the model group (P>0.05).

Effects of Tuina on the Expressions of PI3K/AKT/mTOR Signaling Pathway-Related Proteins in Knee Cartilage Tissues of KOA Rats

Results of Western blot analysis of PI3K, AKT, mTOR, BCL-2, Bax, Beclin1, ULK1, LC3I, LC3II, and LC3II/I in the knee cartilage of rats in each group are shown in Figure 8. As depicted in Figure 9, compared to the blank group, the protein expression of PI3K, AKT, mTOR, and Bcl-2 in the model control group was significantly decreased (P<0.05), and the protein expression of Bax, Beclin1, ULK1, LC3I, LC3II, and LC3II/I was significantly increased (P<0.05).

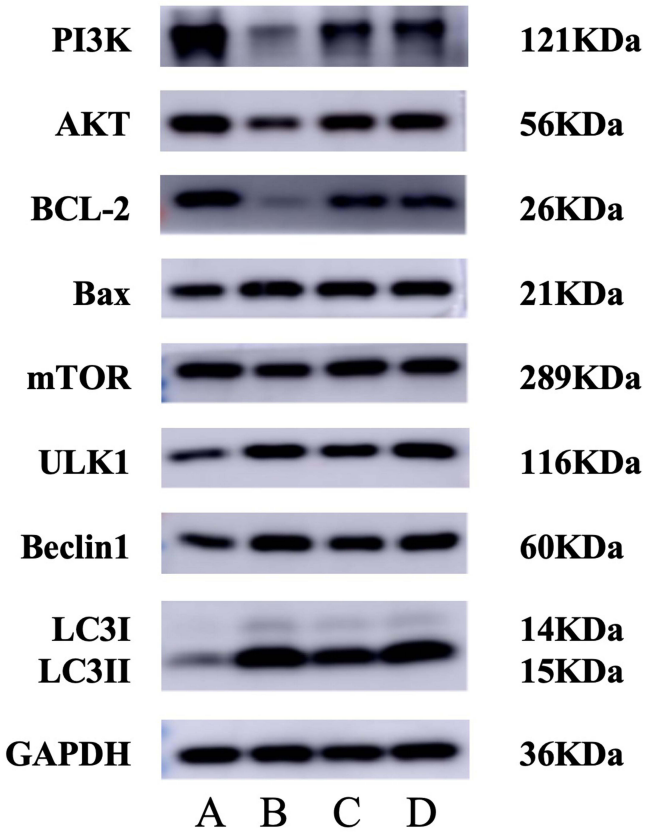

Figure 8 Results of Western blot of PI3K, AKT, mTOR, BCL-2, Bax, Beclin1, ULK1, LC3I, LC3II and LC3II/I in knee cartilage of rats in each group.
Notes: A, blank group; B, model control group; C, Tuina group; D, positive drug group.

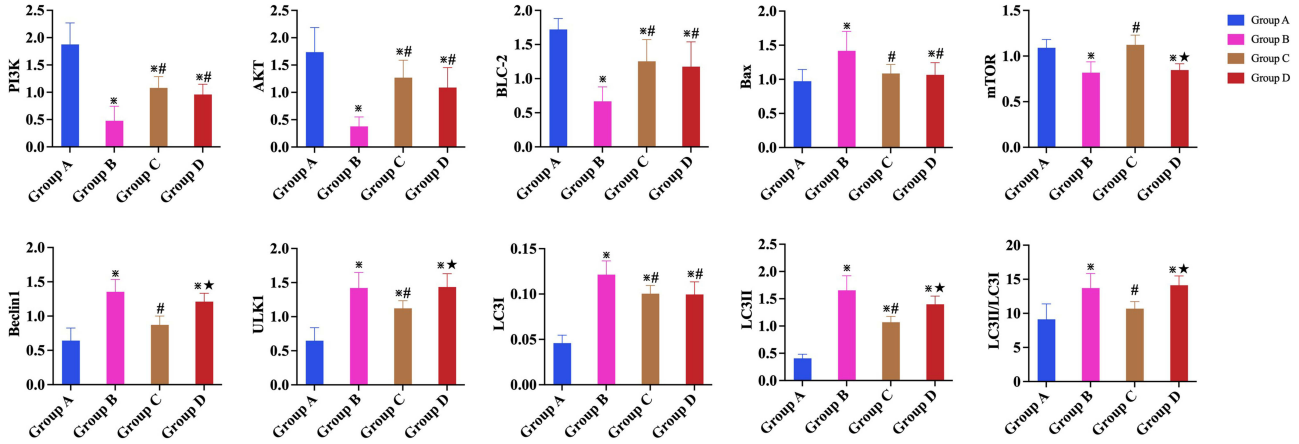

Figure 9 Effects of Tuina on the Expressions of PI3K/AKT/mTOR Signaling Pathway-Related Proteins in Knee Cartilage Tissues of KOA Rats. The protein expression of PI3K, AKT, mTOR, BCL-2, Bax, Beclin1, ULK1, LC3I, LC3II and LC3II/I in knee cartilage of rats in each group was qualified.
Notes: The ordinate is the protein expression of each indicator. Group A, blank group; Group B, model control group; Group C, Tuina group; Group D, positive drug group. ※ Compared with group A, P<0.05; # Compared with group B, P<0.05; ★ Compared with group C, P<0.05.

Compared with the model group, the protein expressions of Bax and LC3I in each treatment group were decreased (P<0.05), while the protein expressions of PI3K, AKT, and BCL-2 were increased (P<0.05). The protein expression of Beclin1, ULK1, LC3II, and LC3II/I, were the lowest (P<0.05), whereas the protein expression of mTOR was the highest in the Tuina group (P<0.05).

Performance of the Random Forest Model

The machine learning results indicated an 83.33% accuracy for the random forest model, remaining stable through both uni- and multivariate analyses. The classification accuracy was supplemented by an F1 score and kappa coefficient. For each label of the four categories, the F1 score value was 1.00, 1.00, 0.80, and 0.67, respectively, with an overall kappa coefficient value of 0.819. The resulting confusion matrix also confirmed the performance of the random forest model (Figure 10).

Feature Importance Analysis

The random forest model determined the significance of various input features in predicting the KOA progression (Figure 11). As the sample size was involved in the Mankin score, the red positive area and red area density were too small, and the machine

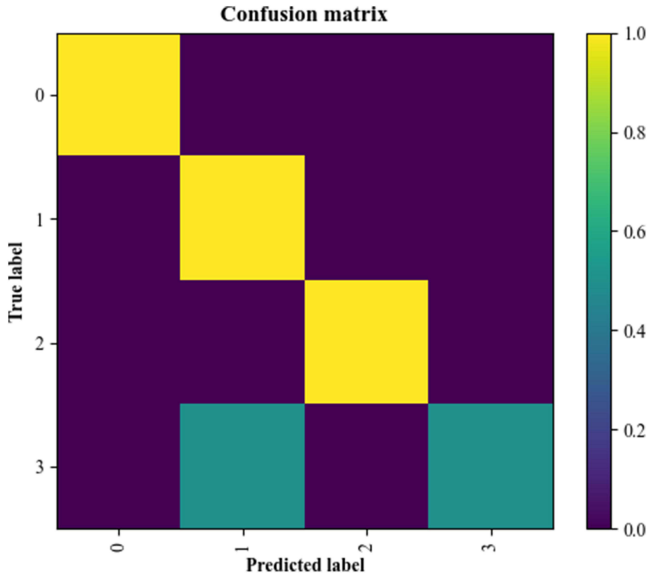

Figure 10 Confusion matrix diagram for model performance.
Notes: The darker the color (from yellow to violet) of the squares in the matrix, the higher the weight of the edges.

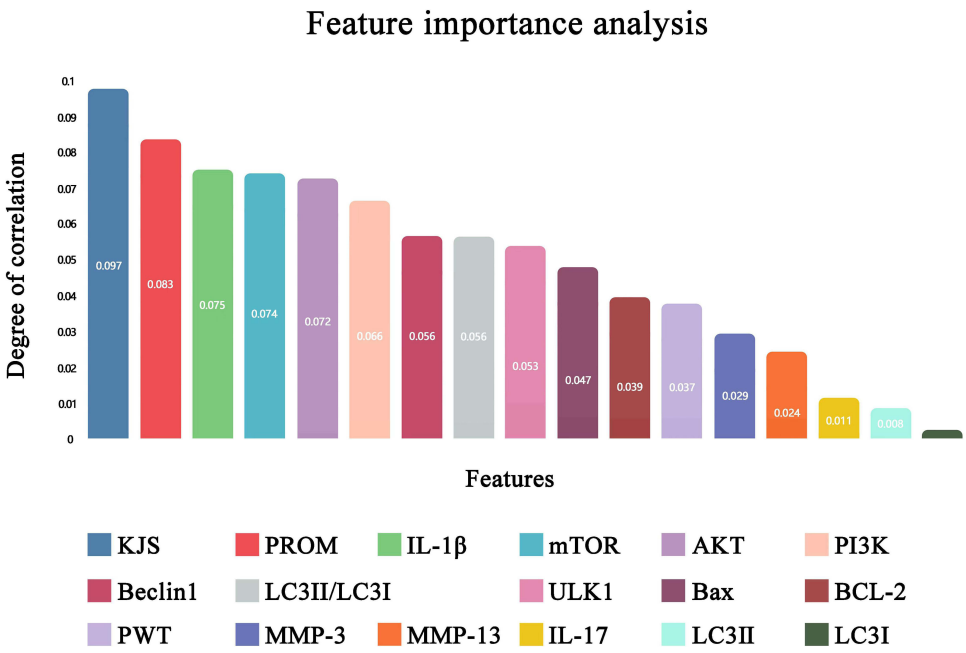

Figure 11 Feature importance score in the random forest model.

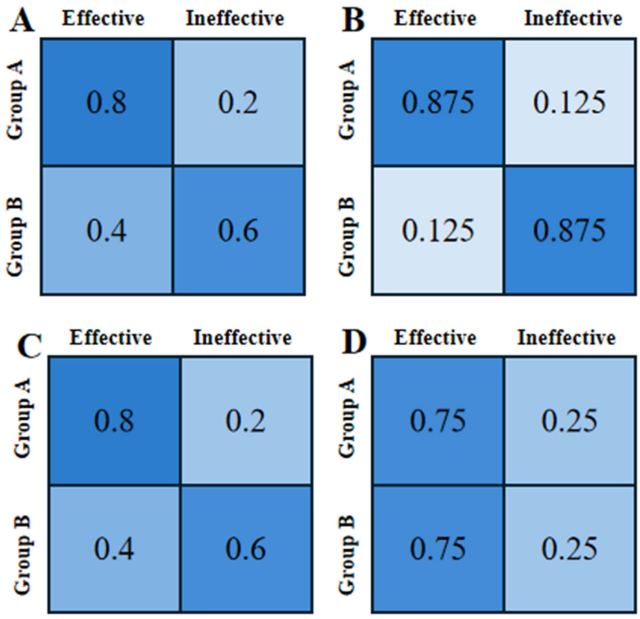

Figure 12 Confusion matrix diagram for curative effect analysis.
Notes: A, overall effect; B, behavioral characteristics; C, PI3K/AKT/mTOR signaling pathway-related metrics; D, cytokines. Group A, Tuina group; Group B, positive drug group.

learning analysis could not be completed. Therefore, these three indicators were not analyzed. Among these, KJS (with a feature importance score of 0.097), PROM (0.083), and IL-1β (0.075) emerged as the three most important predictors. The remaining features ranked in importance as follows: mTOR (0.074), AKT (0.072), PI3K (0.066), Beclin1 (0.056), LC3II/LC3I (0.056), ULK1 (0.053), Bax (0.047), BCL-2 (0.039), PWT (0.037), MMP-3 (0.029), MMP-13 (0.024), IL-17 (0.011), LC3II (0.008), and LC3I (0.002).

Comprehensive and Classified Curative Effect Analysis

The confusion matrix was drawn to visually judge the effect of the massage and positive drug groups in the KOA treatment. As Figure 12A indicates, the comprehensive analyses of all the included features revealed that the overall effect of Tuina on KOA was superior to that of positive drugs. In addition, feature indicators were classified and analyzed in three categories: behavioral characteristics, PI3K/AKT/mTOR-related features, and cytokines. As presented in Figure 12B and C, the capacity of Tuina to improve the behavioral and PI3K/AKT/mTOR signaling pathway-related metrics was superior to that of celecoxib. The cytokine improvement capacity of both groups in KOA rats was consistent after the Tuina and positive drug treatments (Figure 12D).

Discussion

KOA is a chronic degenerative joint disease characterized by low-level inflammation and cartilage degeneration, posing significant challenges in treatment and adversely impacting patients' quality of life.[41] Clinical trials attest to the efficacy of Tuina in improving KOA symptoms, necessitating further exploration of its mechanism.[42,43]

To clarify the potential mechanisms of Tuina, we induced a rat model of KOA using L-cysteine-activated papain injection, observing knee joint cartilage changes. This model, utilizing papain to decompose proteoglycan in the cartilage matrix, mimics early human KOA changes.[44,45] This modeling method has characteristics similar to human KOA and is a better method for studying KOA.

This study targeted two pairs of "Complementary Acupoints", namely Dubi and Nexiyan, Yinlingquan, and Yanglingquan. These pairs of acupoints are located on the yin and yang meridians, opposite each other. The "Complementary Acupoints" embody the TCM theory of "conducting yin from yang, and conducting yang from yin." The Neixiyan point, opposite the Dubi point, is located in the medial recess of the patellar ligament. These points are often used together and are widely used in the treatment of KOA pain with poor flexion and extension.

Electroacupuncture at Dubi and Nexiyan acupoints can alleviate synovial inflammation and delay cartilage degeneration through the TLR4/MyD88/NF-κB signaling pathway.[46] Yanglingquan is located on the lateral side of the knee joint and is Yang, while Yinlingquan is located on the medial side of the knee joint and is called Yin. These acupoints, one inside and one outside, one water and one earth, complement each other, and pressing the two acupoints together alleviates swelling and pain by activating channels and relieving tendons. Additionally, we performed flexion and extension operations on rat knee joints, which helped adjust the force line of the hind limb and changed the internal stress of the knee joint.[47]

Tuina and celecoxib significantly improved the PWT value and knee swelling compared to the model group. Tuina and celecoxib were equally effective in improving PWT; however, Tuina was superior to celecoxib in reducing swelling. Compared with the model group, celecoxib had no significant effect, whereas Tuina treatment significantly improved the PROM of KOA rats. This indicates that both Tuina and celecoxib have obvious analgesic effects, while Tuina is more effective in reducing swelling and improving functional activity.

The HE staining results revealed varying degrees of cartilage degeneration in all groups except the blank group, affirming successful KOA modeling. In the model group, the articular cartilage surface was damaged, with disordered arrangement and necrosis of chondrocytes and the unclear tide line. After celecoxib administration, articular cartilage surface damage in rats was milder. Although the surface was not smooth, it showed potential repair; the chondrocytes are slightly increased, and the cartilage matrix is slightly uneven. After the Tuina treatment, the articular cartilage surface remained smooth and morphologically intact. The number of cells increased compared to the positive drug group, clusters of cell masses were observed, chondrocytes were neatly arranged in the matrix and evenly distributed, and the tide line was slightly incomplete. The quantitative results of the Mankin scores showed that both the Tuina and positive drug groups were significantly lower than those in the model group, and the Tuina group was superior to the positive drug group in terms of reducing Mankin scores. Therefore, it was preliminarily determined that Tuina may help promote cartilage repair and reduce cartilage damage.

Cartilage degeneration is the most significant pathological change associated with KOA.[48] Serum MMP-3 and MMP-13 levels positively correlated with the severity of cartilage degeneration. IL-1β and IL-17, as pro-inflammatory factors regulate inflammatory response and control the degradation of articular cartilage matrix, making them the main targets for treatment.[49,50] This study revealed a notable increase in the levels of inflammatory cytokines and matrix metalloproteinase, such as IL-1β, IL-17, MMP-3, and MMP-13, in rats with KOA. Intervention with Tuina and the positive drug resulted in decreased levels of MMP-3, MMP-13, and pro-inflammatory factors compared to the model group. Additionally, Tuina was comparably effective as a positive drug in improving IL-1β and IL-17, and was more effective in reducing MMP-3 and MMP-13. After analyzing the correlation between these indicators and behavioral indicators, both the Tuina and positive drug groups had significant analgesic effects, likely due to the regulation of inflammatory factors IL-1β and IL-17. Moreover, Tuina's superior improvement in functional activities may be attributed to its regulation of MMP-3 and MMP-13. Tuina reduced the production of MMPs and suppressed the release of pro-inflammatory factors, alleviating cartilage damage.

Abnormal apoptosis and autophagy in chondrocytes are key factors in KOA development.[51] Following the onset of KOA, abnormalities in apoptosis and autophagy disrupt chondrocyte synthesis and metabolism of chondrocytes, limiting the secretion of extracellular matrix crucial for cartilage function, ultimately accelerating cartilage destruction.[52,53] Extensive studies have implicated the involvement of the PI3K/AKT/mTOR pathway in KOA pathogenesis; activation of this pathway regulates the secretion of crucial factors related to chondrocyte apoptosis and autophagy.[54] Additionally, serum MMP and inflammatory factor levels are closely linked to the PI3K/AKT/mTOR signaling pathway.[55] These findings underscore the significance of the PI3K/AKT/mTOR pathway in driving apoptosis and autophagy, contributing to cartilage destruction and KOA progression. Targeting this pathway holds promise in treating or preventing KOA.

In the model group, there was a significant decrease in the gene and protein levels of PI3K, AKT, and mTOR in the cartilage, suggesting inhibition of the PI3K/AKT/mTOR signaling pathway. Notably, Tuina reversed this trend. Bcl-2 and Bax exist in cellular homeostasis as heterodimers and jointly regulate apoptosis. Tuina and positive drug intervention increased Bcl-2 gene and protein expression and decreased Bax gene and protein expression similarly. TUNEL assay results also confirmed their ability to inhibit chondrocyte apoptosis. Activation of the mTOR pathway increases the

attraction to ULK1Ser757 site and stabilizes ULK1, reducing excessive autophagy.[56] Beclin-1 regulates autophagosome synthesis and maturation.[57] LC3 as a specific autophagy marker When autophagy is activated, LC3-I binds to phosphatidyl acetoolamine on the surface of autophagy vesicles to form LC3-II, and the strength of autophagy can be measured by calculating the ratio of LC3-II/LC3-I.[58] Tuina elevated mTOR levels and reduced Beclin1, ULK1, and LC3II/I levels. The positive drug group had no significant effect on autophagy-related indicators.

After analyzing all indicators, Tuina and the positive control drug had similar effects on improving pain symptoms in KOA rats, possibly through regulating inflammatory factors and apoptosis. Tuina improves functional activities, likely due to restored autophagy function through the activated mTOR signaling pathway, leading to reduced secretion of MMPs.

Considering the poor overall prediction of the animal experiments, the random forest model is used to verify and supplement the related findings. The random forest model performed well, proving that the indicators selected in the animal experiment are feasible and reasonable. Our study revealed that KJS, PROM, and IL-1β play are important in the model prediction of KOA regression. The higher KJS and IL-1β and the lower PROM, reportedly the more severe the KOA degree.[59,60] Our results related to these three measures are consistent with those of previous studies. In addition, our discoveries highlight the importance of most PI3K/AKT/mTOR signaling pathway-related indicators as KOA outcome predictors, aligning with the findings of other studies. Reportedly, only LC3II/LC3I is a more accurate predictor and the application of LC3II and LC3I alone allows for limited judgment, which coincides with our results.[61,62]

Forest integration used the majority voting method to evaluate the recovery effect of the Tuina and positive drug groups after treatment. The results indicated that the overall effect of Tuina on KOA was superior to that of positive drugs, thereby highlighting that Tuina exhibited a stronger comprehensive ability to improve KOA-related indicators. In addition, the therapeutic effect of Tuina was affirmed by the performance of each categorical feature. Tuina were superior to celecoxib in all aspects, except for improving cytokines, where Tuina and celecoxib were comparable. Comprehensive analyses revealed that the efficacy results of machine learning were overall consistent with those of rat animal experiments. This machine learning study affirms the rationality of the metrics selected for the in vivo rat experiment and confirms the results obtained from it.

Conclusion

Taken together, by targeting the activation of the PI3K/AKT/mTOR pathway, Tuina could regulate chondrocyte apoptosis and autophagy, inhibit the secretion of inflammatory factors and MMPs, alleviate the inflammatory response, reduce osteoarticular cartilage degeneration, promote cartilage repair, and improve the prognosis of KOA rats. Future research should focus on extending the animal model results to human clinical treatments, which will enhance the practical application of our findings in this study.

Abbreviations

KOA, knee osteoarthritis; SD, Sprague Dawley; PWT, paw withdrawal threshold; PROM, passive range of motion; HE, hematoxylin and eosin; interleukin-1β, IL-1β; matrix metalloproteinase, MMP; ELISA, enzyme-linked immunosorbent assay; RT-qPCR, reverse transcription-quantitative polymerase chain reaction; PI3K/AKT/mTOR, phosphoinositide 3-kinase/protein kinase B/mammalian target of rapamycin; ECM, extracellular matrix; TCM, traditional Chinese medicine.

Data Sharing Statement

The datasets used and/or analyzed during the current study are available from the corresponding author on reasonable request.

Ethics Approval and Consent to Participate

This study was approved by the Ethics Committee of Henan University of Traditional Chinese Medicine (Approval number: IACUC-202309024). All experiments were conducted in accordance with the National Institutes of Health's Guidelines for the Care and Use of Laboratory Animals.

Consent for Publication

All authors consent to publish this manuscript.

Acknowledgments

We acknowledge their professors and classmates at the Acupuncture-Moxibustion and Tuina School of Henan University of Chinese Medicine for their generous guidance and assistance.

Author Contributions

Zhen Wang, Hui Xu, Zheng Wang and Yu Wang have contributed equally to this work and share first authorship. All authors made a significant contribution to the work reported, whether that is in the conception, study design, execution, acquisition of data, analysis and interpretation, or in all these areas; took part in drafting, revising or critically reviewing the article; gave final approval of the version to be published; have agreed on the journal to which the article has been submitted; and agree to be accountable for all aspects of the work.

Funding

This work was supported by the Henan Province Chinese Medicine Scientific Research Special project (No. 2024ZY3060), the Central Plains Thousand Talents Program-Central Plains Famous Doctors (No. ZYQR201912120), the 2022 Central Plains Talent Plan (Talent Education Series)-Central Plains Youth Top Talent Project (No. Yu Talent Office [2022] No. 5), the Henan Province Science and Technology Research-Social Development Project (No. 222102310214), the Henan Provincial Science and Technology R&D Program Joint Fund (superior discipline cultivation category) (No. 222301420061), the 2022 henan Province Traditional Chinese Medicine Scientific Research Project (No. 2022ZY2023), Henan Province Key Research and Development and Promotion Special Project (Science and Technology Research)(No. 232102311203), Henan University of Chinese Medicine graduate research innovation ability improvement plan project (2023KYCX071), and Henan Province Traditional Chinese Medicine "Double First-Class" Scientific Research Project (No. HSRP-DFCTCM-2023-7-09).

Disclosure

The authors declare no competing interests.

References

1. Katz JN, Arant KR, Loeser RF. Diagnosis and treatment of hip and knee osteoarthritis: a review. *JAMA*. 2021;325(6):568–578. doi:10.1001/jama.2020.22171
2. Jang S, Lee K, Ju JH. Recent updates of diagnosis, pathophysiology, and treatment on osteoarthritis of the knee. *Int J Mol Sci*. 2021;22(5):2619. doi:10.3390/ijms22052619
3. Giorgino R, Albano D, Fusco S, Peretti GM, Mangiavini L, Messina C. Knee osteoarthritis: epidemiology, pathogenesis, and mesenchymal stem cells: what else is new? An update. *Int J Mol Sci*. 2023;24(7):6405. doi:10.3390/ijms24076405
4. Bijlsma JW, Berenbaum F, Lafeber FP. Osteoarthritis: an update with relevance for clinical practice. *Lancet*. 2011;377(9783):2115–2126. doi:10.1016/S0140-6736(11)60243-2
5. Michael JW, Schlüter-Brust KU, Eysel P. The epidemiology, etiology, diagnosis, and treatment of osteoarthritis of the knee. *Dtsch Arztebl Int*. 2010;107(9):152–162. doi:10.3238/arztebl.2010.0152
6. Sowers MR, Karvonen-Gutierrez CA. The evolving role of obesity in knee osteoarthritis. *Curr Opin Rheumatol*. 2010;22(5):533–537. doi:10.1097/BOR.0b013e32833b4682
7. Kulkarni K, Karssiens T, Kumar V, Pandit H. Obesity and osteoarthritis. *Maturitas*. 2016;89:22–28. doi:10.1016/j.maturitas.2016.04.006 PMID: 27180156.
8. Page CJ, Hinman RS, Bennell KL. Physiotherapy management of knee osteoarthritis. *Int J Rheum Dis*. 2011;14(2):145–151. doi:10.1111/j.1756-185X.2011.01612.x
9. Roos EM, Arden NK. Strategies for the prevention of knee osteoarthritis. *Nat Rev Rheumatol*. 2016;12(2):92–101. doi:10.1038/nrrheum.2015.135
10. Pesare E, Vicenti G, Kon E, et al. Italian Orthopaedic and Traumatology Society (SIOT) position statement on the non-surgical management of knee osteoarthritis. *J Orthop Traumatol*. 2023;24(1):47. doi:10.1186/s10195-023-00729-z
11. Guo JY, Li F, Feng YR. Chinese rehabilitation guide for knee osteoarthritis (2023 edition). *Chinese J of Evidence-Based Med*. 2024;24(01):1–14.
12. Xu XM, Liu WG, Xu SC, et al. Clinical practice guide of integrated Chinese and western medicine for knee osteoarthritis. *J Pract Med*. 2021;37(22):2827–2833.
13. Song X, Liu Y, Chen S, et al. Knee osteoarthritis: a review of animal models and intervention of traditional Chinese medicine. *Animal Model Exp Med*. 2024;7(2):114–126. doi:10.1002/ame2.12389

14. Xu H, Zhao C, Guo G, et al. The effectiveness of tuina in relieving pain, negative emotions, and disability in knee osteoarthritis: a randomized controlled trial. *Pain Med*. 2023;24(3):244–257. doi:10.1093/pm/pnac127
15. Xu H, Xie J, Xiao LB, et al. Clinical observation on joint treatment of pain of knee osteoarthritis with local acupoint and sitting position. *World Sci Tech Modernization of Tradition Chin Med*. 2021;23(06):2125–2131.
16. Xu H, Kang BX, Zhong S, et al. Joint treatment of knee osteoarthritis with local acupoints and sitting position: a randomized controlled study. *J Tissue Eng*. 2021;25(02):216–221.
17. Guilak F, Nims RJ, Dicks A, Wu CL, Meulenbelt I. Osteoarthritis as a disease of the cartilage pericellular matrix. *Matrix Biol*. 2018;71-72:40–50. doi:10.1016/j.matbio.2018.05.008
18. Liu Y, Xu S, Zhang H, et al. Stimulation of α7-nAChRs coordinates autophagy and apoptosis signaling in experimental knee osteoarthritis. *Cell Death Dis*. 2021;12(5):448. doi:10.1038/s41419-021-03726-4
19. Lorenzo-Gómez I, Nogueira-Recalde U, García-Domínguez C, et al. Defective chaperone-mediated autophagy is a hallmark of joint disease in patients with knee osteoarthritis. *Osteoarthritis Cartilage*. 2023;31(7):919–933. doi:10.1016/j.joca.2023.02.076
20. Zheng LJ, Wang K, Li MZ, Wang JM, Qiao YJ, Li HD. Shutiaojing massage can maintain the stability of the internal environment of rabbit cartilage cells damaged by knee osteoarthritis. *J Tissue Eng*. 2023;27(35):5681–5687.
21. Wang K, Chu M, Wang F, Zhao Y, Chen H, Dai X. Putative functional variants of PI3K/AKT/mTOR pathway are associated with knee osteoarthritis susceptibility. *J Clin Lab Anal*. 2020;34(6):e23240. doi:10.1002/jcla.23240
22. Xu K, He Y, Moqbel SAA, Zhou X, Wu L, Bao J. SIRT3 ameliorates osteoarthritis via regulating chondrocyte autophagy and apoptosis through the PI3K/Akt/mTOR pathway. *Int J Biol Macromol*. 2021;175:351–360. doi:10.1016/j.ijbiomac.2021.02.029
23. Sun K, Luo J, Guo J, Yao X, Jing X, Guo F. The PI3K/AKT/mTOR signaling pathway in osteoarthritis: a narrative review. *Osteoarthritis Cartilage*. 2020;28(4):400–409. doi:10.1016/j.joca.2020.02.027
24. Ersahin T, Tuncbag N, Cetin-Atalay R. The PI3K/AKT/mTOR interactive pathway. *Mol Biosyst*. 2001;11(7):1946–1954. doi:10.1039/c5mb00101c
25. Badyal DK, Desai C. Animal use in pharmacology education and research: the changing scenario. *Indian J Pharmacol*. 2014;46(3):257–265. doi:10.4103/0253-7613.132153
26. Handelman GS, Kok HK, Chandra RV, Razavi AH, Lee MJ, Asadi H. eDoctor: machine learning and the future of medicine. *J Intern Med*. 2018;284(6):603–619. doi:10.1111/joim.12822
27. Rauschert S, Raubenheimer K, Melton PE, Huang RC. Machine learning and clinical epigenetics: a review of challenges for diagnosis and classification. *Clin Clin Epigenet*. 2020;12(1):51. doi:10.1186/s13148-020-00842-4
28. Gelbard RB, Hensman H, Schobel S, et al. A random forest model using flow cytometry data identifies pulmonary infection after thoracic injury. *J Trauma Acute Care Surg*. 2023;95(1):39–46. doi:10.1097/TA.0000000000003937
29. Cheng L, Huang C, Li M, Shang S, Chen J, Tang Z. Chonggu granules improve cartilage matrix metabolism in knee osteoarthritis via the miR-148a-3p/Wnt/β-catenin pathway. *J Inflamm Res*. 2023;16:4751–4762. doi:10.2147/JIR.S428582
30. Ye JM, Liang ZC. Comparison of three different methods of knee osteoarthritis modeling. *Chin J Gerontol*. 2023;43(16):3948–3954.
31. Zhou JH, Wu YZ, Li SS, Zhu WM, Zhang SH. Evaluation of knee osteoarthritis model in rats. *Chin J Tissue Engg Res Clin Rehabil*. 2010;14(33):6206–6209.
32. Lee YJ, Park JA, Yang SH, et al. Evaluation of osteoarthritis induced by treadmill-running exercise using the modified Mankin and the new OARSI assessment system. *Rheumatol Int*. 2011;31(12):1571–1576. doi:10.1007/s00296-010-1520-4
33. Song BL, Yu TY Therapeutics of Chinese Tuina. Beijing: People's Medical Publishing House; 2016:165–171.
34. Guo Y. *Map of Acupuncture and Moxibustion Acupuncture Points for Laboratory Animals*. Beijing: China Traditional Chinese Medicine Press; 2023:321–329.
35. Nayarisseri A, Khandelwal R, Tanwar P, et al. Artificial intelligence, big data and machine learning approaches in precision medicine & drug discovery. *Curr Drug Targets*. 2021;22(6):631–655. doi:10.2174/1389450122999210104205732
36. Wallace ML, Mentch L, Wheeler BJ, et al. Use and misuse of random forest variable importance metrics in medicine: demonstrations through incident stroke prediction. *BMC Med Res Methodol*. 2023;23(1):144. doi:10.1186/s12874-023-01965-x
37. Hu J, Szymczak S. A review on longitudinal data analysis with random forest. *Brief Bioinform*. 2023;24(2):bbad002. doi:10.1093/bib/bbad002
38. Yao W, Frydman H, Larocque D, Simonoff JS. Ensemble methods for survival function estimation with time-varying covariates. *Stat Methods Med Res*. 2022;31(11):2217–2236. doi:10.1177/09622802221111549
39. Das J, Kumar S, Mishra DC, Chaturvedi KK, Paul RK, Kairi A. Machine learning in the estimation of CRISPR-Cas9 cleavage sites for plant system. *Front Genet*. 2023;13:1085332. doi:10.3389/fgene.2022.1085332
40. Zhang YY, Zhao HS, Sun YF, Lu BW, Sun L. Development and validation of biomarkers related to PANoptosis in osteoarthritis. *Eur Rev Med Pharmacol Sci*. 2023;27(16):7444–7458. doi:10.26355/eurrev_202308_33396 PMID: 37667921.
41. Kobayashi S, Pappas E, Fransen M, Refshauge K, Simic M. The prevalence of patellofemoral osteoarthritis: a systematic review and meta-analysis. *Osteoarthritis Cartilage*. 2016;24(10):1697–1707. doi:10.1016/j.joca.2016.05.011
42. Wang CP, Liang Y, Yu WJ, Sha H, Cheng SM. Clinical effect and mechanical mechanism of acupoint kneading and massage in treatment of straightening disorder of knee osteoarthritis. *J Mod Int Chin Western Med*. 2023;32(08):1080–1085.
43. Huang JM, Lin Z, Zheng LB, Wang G, Long XY. Jian xiang Daniel reinforcement type massage points make a diagnosis and give treatment of knee osteoarthritis clinical observation. *J Massage Rehabil Med*. 2023;14(02):13–16.
44. Ghouri A, Muzumdar S, Barr AJ, et al. The relationship between meniscal pathologies, cartilage loss, joint replacement and pain in knee osteoarthritis: a systematic review. *Osteoarthritis Cartilage*. 2022;30(10):1287–1327. doi:10.1016/j.joca.2022.08.002
45. Driban JB, Harkey MS, Barbe MF, et al. Risk factors and the natural history of accelerated knee osteoarthritis: a narrative review. *BMC Musculoskelet Disord*. 2020;21(1):332. doi:10.1186/s12891-020-03367-2
46. Zhou ZQ, Yang YJ, Ma XD, Zhang SY, Guan XF. Mechanism of electroacupuncture through TLR4/MyD88/NF-κB signaling pathway to improve synovitis response in knee osteoarthritis. *Acupuncture Res*. 2023;48(04):353–358+365. doi:10.13702/j.1000-0607.20220418
47. Kang ZR, Gong L, Xing H, Dai DC. A preliminary study on the therapeutic concept and principle of sitting knee adjustment in the treatment of knee osteoarthritis. *J Shanghai Univ Traditional Chin Med*. 2019;34(04):98–102.
48. Eagle S, Potter HG, Koff MF. Morphologic and quantitative magnetic resonance imaging of knee articular cartilage for the assessment of post-traumatic osteoarthritis. *J Orthop Res*. 2017;35(3):412–423. doi:10.1002/jor.23345

49. Chen JJ, Shang SS, Li M, Huang CB. Effects of chonggu granules on IL-17, IL-35 cytokines and cartilage matrix metabolism in knee osteoarthritis. *Chin J Osteoporosis*. 2023;29(03):397–402.
50. Xiong A, Wei XY, Xu JZ, Luo F. Expression and significance of HIF-1α, OPN, IL-1β, TNF-α, MMP-13 and NGF protein in SD rats with knee osteoarthritis induced by monosodium iodoacetate. *Chin J Exp Anim Sci*. 2023;31(05):643–652.
51. Feng L, Feng C, Wang CX, et al. Circulating microRNA let-7e is decreased in knee osteoarthritis, accompanied by elevated apoptosis and reduced autophagy. *Int J Mol Med*. 2020;45(5):1464–1476. doi:10.3892/ijmm.2020.4534
52. Sasaki H, Takayama K, Matsushita T, et al. Autophagy modulates osteoarthritis-related gene expression in human chondrocytes. *Arthritis Rheum*. 2012;64(6):1920–1928. doi:10.1002/art.34323
53. Wang XJ, Tian W, Xu WW, et al. Loss of Autophagy Causes Increased Apoptosis of Tibial Plateau Chondrocytes in Guinea Pigs with Spontaneous Osteoarthritis. *Cartilage*. 2021;13(2_suppl):796S–807S. doi:10.1177/19476035211044820
54. Da-Wa ZX, Jun M, Chao-Zheng L, et al. Exosomes derived from M2 macrophages exert a therapeutic effect via inhibition of the PI3K/AKT/mTOR pathway in rats with knee osteoarthritic. *Biomed Res Int*. 2021;2021:7218067. doi:10.1155/2021/7218067
55. Zhang Y, Liang J, Cao N, et al. ASIC1α up-regulates MMP-2/9 expression to enhance mobility and proliferation of liver cancer cells via the PI3K/AKT/mTOR pathway. *BMC Cancer*. 2022;22(1):778. doi:10.1186/s12885-022-09874-w
56. Huang H, Wang T, Wang L, et al. Saponins of Panax japonicus ameliorates cardiac aging phenotype in aging rats by enhancing basal autophagy through AMPK/mTOR/ULK1 pathway. *Exp Gerontol*. 2023;182:112305. doi:10.1016/j.exger.2023.112305
57. Zhang XW, Wu NP, Zhou CF, Tang JF. Research progress of Beclin1 in autophagy and its protein modification. *Chin J Biol*. 2023;36(6):751–758+763.
58. Ji Y, Xiong L, Zhang G, et al. Synovial fluid exosome-derived miR-182-5p alleviates osteoarthritis by downregulating TNFAIP8 and promoting autophagy through LC3 signaling. *Int Immunopharmacol*. 2023;125(Pt A):111177. doi:10.1016/j.intimp.2023.111177
59. Sari Z, Aydoğdu O, Demirbüken I, Yurdalan SU, Polat MG. A better way to decrease knee swelling in patients with knee osteoarthritis: a single-blind randomised controlled trial. *Pain Res Manag*. 2019;2019:8514808. doi:10.1155/2019/8514808
60. He L, He T, Xing J, et al. Bone marrow mesenchymal stem cell-derived exosomes protect cartilage damage and relieve knee osteoarthritis pain in a rat model of osteoarthritis. *Stem Cell Res Ther*. 2020;11(1):276. doi:10.1186/s13287-020-01781-w
61. Kurakazu I, Akasaki Y, Tsushima H, et al. TGFβ1 signaling protects chondrocytes against oxidative stress via FOXO1-autophagy axis. *Osteoarthritis Cartilage*. 2021;29(11):1600–1613. doi:10.1016/j.joca.2021.07.015
62. Wu SY, Du YC, Yue CF. Sirt7 protects chondrocytes degeneration in osteoarthritis via autophagy activation. *Eur Rev Med Pharmacol Sci*. 2020;24(18):9246–9255. doi:10.26355/eurrev_202009_23006